Investigation of Metallography and Behavior of M-A Constituent in Weld HAZ of HSLA Steels†

Ivan HRIVNAK*, Fukuhisa MATSUDA, Zhonglin LI***, Kenji IKEUCHI**** and Hitoshi OKADA*******

Abstract

The metallography of M-A constituent was investigated in simulated underbead zone of HT 80 and HT 100 QT steels. It was found that M-A consistsed of cementite precipitated from retained austenite, structurally free cementite precipitated from lath martensite during its self-tempering, lath martensite, plate martensite and small portion of retained austenite. Investigation was also made of the effect of M-A on the deformation and fracture behaviors of specimens. M-A deteriorated the ductility of HAZ by initiation of dimpled fracture. Dimples could initiate from microvoids coalescence at the interface between M-A and matrix and further on cracked or fragmented M-A particles. M-A could contribute to cleavage fracture propagation by reinitiating the fracture. Elongated and massive M-A constituent were found in steels investigated.

KEY WORDS :(High Strength Steel) (Weld Simulation) (Decomposition) (M-A Constituent) (Ductility) (Impact Properties)

1. Introduction

The weldability of high strength steel is influenced by many factors, but the main among them are the steel chemistry and its mode of production. Advances in metallurgy make it possible to produce high strength steels with low carbon content and carbon equivalent value, which have high purity and very fine grains. The weldability of such steels is very good unless high heat inputs are used in welding. In that case, a structure degradation due to strong alloy effect on transformation sequences occurs at compositions which normally would have produce excellent impact properties. At slower cooling rates, the microstructure of the HAZ changes from martensite to lower bainite, upper or granular bainite as described by Habraken and Economopoulos[1]. Granular bainite has a composite microstructure of bainitic ferrite together with retained austenite and martensite. Granular bainite is free from cementite, and ferrite in it has a lath like morphology. In bainite matrix, an inhomogeneous distribution of retained austenite is observed. Sometimes it forms small island, but it may be also deposited in the form of thin films between the ferrite laths. The retained austenite may partly transform during the cooling to martensite. Verrier et al.[2] described the side plate structure with carbide colonies and/or M-A (Martensite-Austenite) islands in between depending on alloy content and heat input. At very low cooling rates, the retained austenite can be partially transformed into pearlite. At higher cooling rates, the predominant transformation product of retained austenite is martensite. The martensite transformation is accomplished with the maximum expenditure of strain energy by a homogeneous distortion of the austenite. The strain can occur either by slip or by twinning. Slip occurs at higher M_S temperatures and twinning at lower M_S temperatures. The orientation relationships of martensite to the parent austenite were described by Kurdjumov and Sachs as follows:

$$\{111\}_\gamma \,//\, \{110\}_\alpha,$$
$$\langle 110\rangle_\gamma \,//\, \langle 111\rangle_\alpha,$$

The common structure of martensite is lath martensite. Inside the laths high dislocation density over 10^{15} m^{-2} is observed. But when the carbon content in austenite to be transformed exceeds $\sim$ 0.4%, the morphology of martensite is changed from lath to plate martensite. Plate martensite has lower M_S temperature, below $\sim$ 473 K, and the laths are internally twinned. According to Speich and Leslie[3] the twins can gradually merge into an array of dislocations near the periphery of the plate. They also concluded that the transition from lath to plate martensite is not abrupt. With increasing carbon content also content of retained austenite is increasing. The presence of retained austenite is considered to be very harmful for the toughness. Concerning the M-A constituent, the volume fraction of γ increases with increasing cooling time, $t_{8/5}$, as a consequence of carbon enrichment from the increment of diffusion time, and usually is close to 2-6% in the HAZ exhibiting upper bainitic structure.

† Received on Oct. 31,1992

* Visiting Professor (Professor, Technical University in Kosice, Kosice, Slovakia)
** Professor
*** Visiting Scientist (Lecturer, Harbin Institute of Technology, Harbin, China)
**** Associate Professor
***** Kurimoto, Ltd., Osaka

Transactions of JWRI is published by Welding Research Institute, Osaka University, Ibaraki, Osaka 567, Japan

According to Verrier et al.[2] the presence of 1% retained austenite will increase the notch toughness transition temperature by 15 K. According to Ikawa et al.[4] retained austenite promotes initiation and propagation of the fracture.

Higher carbon content in M-A constituent was found by many authors. Recently Josefsson and Andren[5] found 1.14%C in M-A comparing with 0.005%C in the surrounding ferrite. Moreover they made a calculation of equilibrium content of carbon in retained austenite. They calculated the temperature-carbon concentration dependence in bainitic reaction and compared the temperatures where the austenite and ferrite of the same composition have the same free energy in a stress free transformation with the temperature which additionally takes the transformation strain energy into account. Further they supposed the diffusion of carbon but no substitutional alloying elements. They concluded that at 693 K where the bainitic reaction ceases, the expected carbon concentration in austenite is about 2.6mass%. In their investigation the bainite start temperature (B_S) was determined to be 851 ± 5 K, but the transformation started at a lower temperature during continuous cooling, between 843 and 693 K. High carbon content is expected also from the (micro)hardness measurements of M-A. Matsuda et al.[6] tried to find a correlation between the carbon content of M-A and its hardness. The carbon content was measured by EPMA both in elongated M-A and in massive M-A in the range of 0.6-2.0%. Hardness of M-A could then be expressed as $H_{M\text{-}A} = 575 \cdot C + 15$. It is known that the hardness of martensite is a function of carbon content only and other alloying elements present in the steel can affect but its hardenability. According to Duren[7] the hardness of martensite can be expressed as $H_M = 802 \cdot C + 305$, or according to Satoh and Terasaki[8] as $H_M = 812 \cdot C + 293$. Recently Yurioka[9] gave for martensite hardness ($C < 0.8\%$) following expression: $H_M = 884 \cdot (1 - 0.3 \cdot C^2) + 294$. Krauss[10] measured the hardness of martensite in wide carbon concentration range, up to 1.1%C, and has found a linear dependence of hardness on carbon content up to ~ 0.6%C: $H_M = 800 \cdot C + 240$, while at high carbon contents the martensite hardness was decreased due to increased portion of retained austenite. From the difference between the measurements of Matsuda et al.[6] and others we can conclude that M-A constituent must have remarkable amount of retained austenite.

Concerning the effect of M-A constituent on ductility and toughness of weld, there is a general agreement that M-A impairs the plasticity of steel. M-A must be considered to be coarse, brittle second phase particles in ferrite. In some papers it is still discussed whether the areas containing M-A constituent have to be regarded as

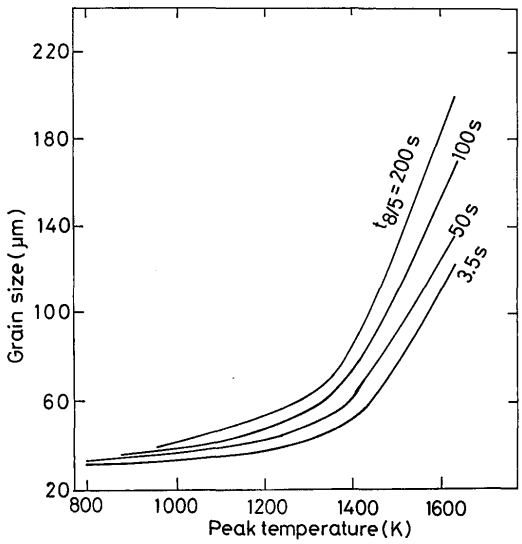

Fig. 1 Effect of peak temperature and cooling time on the austenite grain size in simulated HAZ of HT 80B.

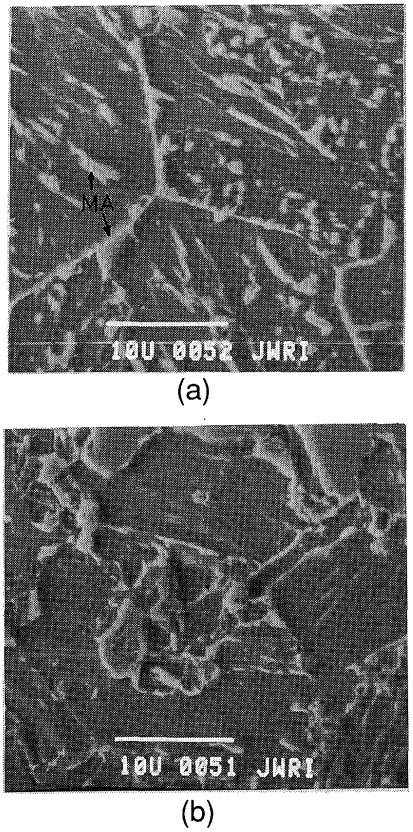

Fig. 2 The appearance of M-A constituent in simulated HAZ of HT 80B (observed with SEM). a) peak temperature = 1623 K, $t_{8/5}$ = 200 s. b) peak temperature = 1013 K, $t_{8/5}$ = 200 s.

Table 1 Chemical composition of the steel plates used (mass%).

Steel	Thickness (mm)	C	Si	Mn	P	S	Cu	Ni	Cr	Mo	V	Nb	Al	B
HT 80A	60	0.12	0.23	0.93	0.006	0.002	0.19	1.22	0.48	0.45	0.03	-	0.066	0.0007
HT 80B	25	0.10	0.27	0.92	0.009	0.002	0.20	0.98	0.47	0.27	0.04	-	0.052	0.0012
HT 100A	150	0.14	0.05	1.03	0.004	0.001	0.23	3.80	0.56	0.58	0.027	0.012	0.047	0.0011
HT 100B	38	0.11	0.11	0.86	0.004	0.001	0.03	1.57	0.54	0.56	0.073	-	0.053	0.0011

LBZ (Local Brittle Zone) or the main reason for the worst toughness is the occurrence of lath upper bainite microstructure[2]. Chen et al.[11] studied the behavior of M-A in tensile tests carried out at different temperatures, and observed high stress concentration on the boundary between α - Fe and M-A constituent. At moderate and high temperatures this stress makes the boundary crack or debond. With increasing strain crack grows to voids and further develops to deep holes. At lower temperatures, however, stiffer blocky M-A gives rise to concentration and triaxiality of stress at the point near the boundary on the side of ferrite and makes the later cleavage crack. Very important is the size of M-A. The larger the size, the smaller is the load to make the new crack nucleus initiate.

Matsuda et al.[6,12] investigated the effect of M-A constituent on the notch toughness energy at room temperature in the simulated HAZ of HT 80 and HT 100 high strength steels. The area fraction of M-A ranged between 0 and 19%. The drop in absorbed energy KV with increasing area fraction of M-A could be expressed as KV(J) = 225 - 12.5(%M-A), or KV(J) = 250 - 11.8(%M-A) for HT 80 steel but no similar relationship was found for HT 100.

2. Experimental Procedures

Although four high strength low alloy steels of HT 80 and HT 100 (each of two types) were used in this investigation, the main research was carried out on HT 80B steel. The chemical composition and plate thickness are presented in **Table 1.**

Simulated weld thermal cycles of underbead zones were conducted by a Gleeble-1500 weld simulator which was based on direct resistance heating. The peak temperature of simulated welding cycle was T_p = 1623 K, soaking time at the peak temperature 6 s and cooling rates, expressed in terms of cooling times between 1073 K and 773 K, $t_{8/5}$, ranged from 3.5 to 200 s. This investigation followed the previous ones[6,12].

3. Experimental Results

3.1 Metallography of M-A Constituent

The effect of the peak temperature and cooling time $t_{8/5}$ on grain size of simulated HAZ is depicted in **Fig. 1**. The γ–grains start to coarsen more rapidly at temperatures above ~1423 K.

The microstructure of the simulated underbead zone of HT 80B, with peak temperature of 1623 K and cooling time $t_{8/5}$ = 200 s is characterized by **Fig. 2a**. The M-A constituent is formed either on grain boundaries or inside the grains. Two shapes of M-A can be resolved: elongated and massive. The plane fraction of M-A in this specimen was 22.6%, from which elongated particles took 5%. Figure 2b shows the microstructure of HT 80B in the simulated intercritical zone subjected to the thermal cycle of the peak temperature of 1013 K and of the cooling time corresponding to $t_{8/5}$ = 200 s. At this peak temperature the transformation $\alpha \rightarrow \gamma$ starts at grain boundaries, and only carbon rich constituents form austenite, while the remainder is unchanged. Which type of constituent would form from the carbon rich austenite is determined by the subsequent cooling rate. In our case, the cooling rate was so slow that the resulting microstructure in transformed islands was composed of upper bainite with the presence of great part of M-A constituent.

From Fig. 2, it is seen that when using 2-4% Nital as etchant, the ferrite matrix is preferentially dissolved and M-A constituent as well as carbides remain undissolved or dissolved at considerable lower rate. When the etching time was prolonged, we could extract the M-A particles into carbon replica. Such case is illustrated in **Fig. 3** in which extracted M-A particles from simulated underbead zone of HT 100B are seen. By electron diffraction we could determine the phase composition of extracted M-A. We have identified cementite, retained austenite and, of course, ferrite (martensite) from which the M-A is composed. In some cases we could also resolve the microtwinned martensite. But usually the lattice imperfection contrast was not satisfactory and was

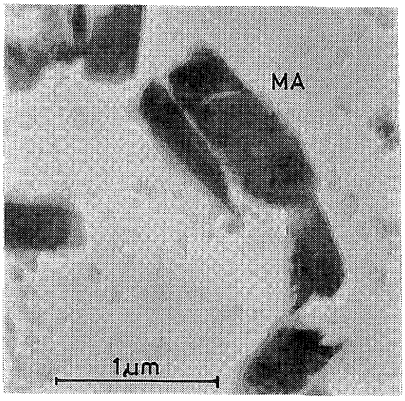

Fig. 3 Extracted M-A particles from simulated HAZ of HT 100B (Extraction carbon replica).

overlapped by variety of extinctions contours. **Figures 4a** and **4b** show an example of M-A-C in HT 80B. Figure 4a is a bright field image obtained from the extracted M-A particle, while Fig. 4b is a dark field image taken from 110 reflection of martensite which nearly coincides with (210) plane of cementite. Electron diffraction identified the presence of ferrite (martensite) and cementite. Inside the M-A a remarkable amount of rod-like cementite was found. From its morphology we can suggest it as a result of lath martensite self-tempering. Besides the very fine cementite we could detect in M-A constituent also coarser cementite parts usually situated at the boundary between M-A and ferrite matrix. An example of such cementite is given in **Fig. 5**, which is from simulated underbead zone of HT 80A. Cementite was identified by electron diffraction. It is supposed that this cementite has precipitated from retained austenite at high temperatures.

When using thin foil technique in transmission electron microscope we could investigate the internal structure of M-A. An example of M-A island surrounded by ferrite is given in **Fig. 6a**. The martensite laths have not uniform orientation, exhibit a high dislocation density and in some parts internal twinning can be resolved. The twins are oriented in $<110>_{\alpha\text{-Fe}}$. At the boundary between martensite and ferrite several cementite particles were detected. From their morphology we can conclude that these carbides were precipitated from austenite. Figure 6b shows similar example of M-A constituent as observed in TEM. In this case we could not find cementite particles in it, but in diffraction spectrum diffraction spots corresponding to austenite were detected. Figure 6c gives an example of the morphology of elongated M-A constituent. In many cases internal structure of M-A could not be resolved. Also in this case, we cannot resolve either martensite laths nor plates (microtwinns). At the boundary between M-A and matrix the presence

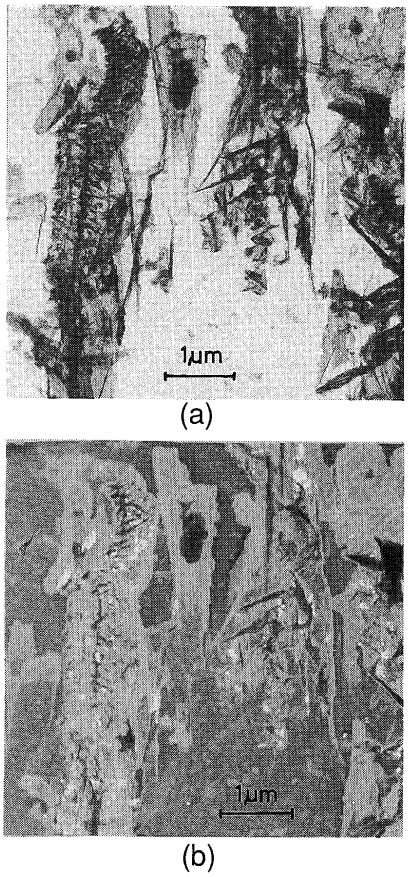

Fig. 4 Bright (a) and dark (b) field images from extracted M-A-C particles in simulated HAZ of HT 80B (operating reflection is $110_{\alpha\text{-Fe}}$).

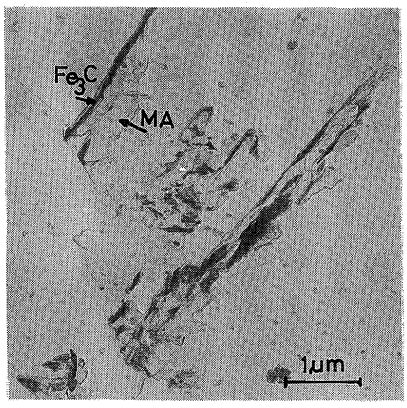

Fig. 5 Morphology of massive M-A particles in simulated HAZ of HT 80A (extraction carbon replica). Dark particles are cementite.

of cementite carbide was recorded. The surrounding ferrite matrix had always high density of dislocations. Other case is recorded in Fig. 6d which was taken from the same specimen. In massive M-A the presence of

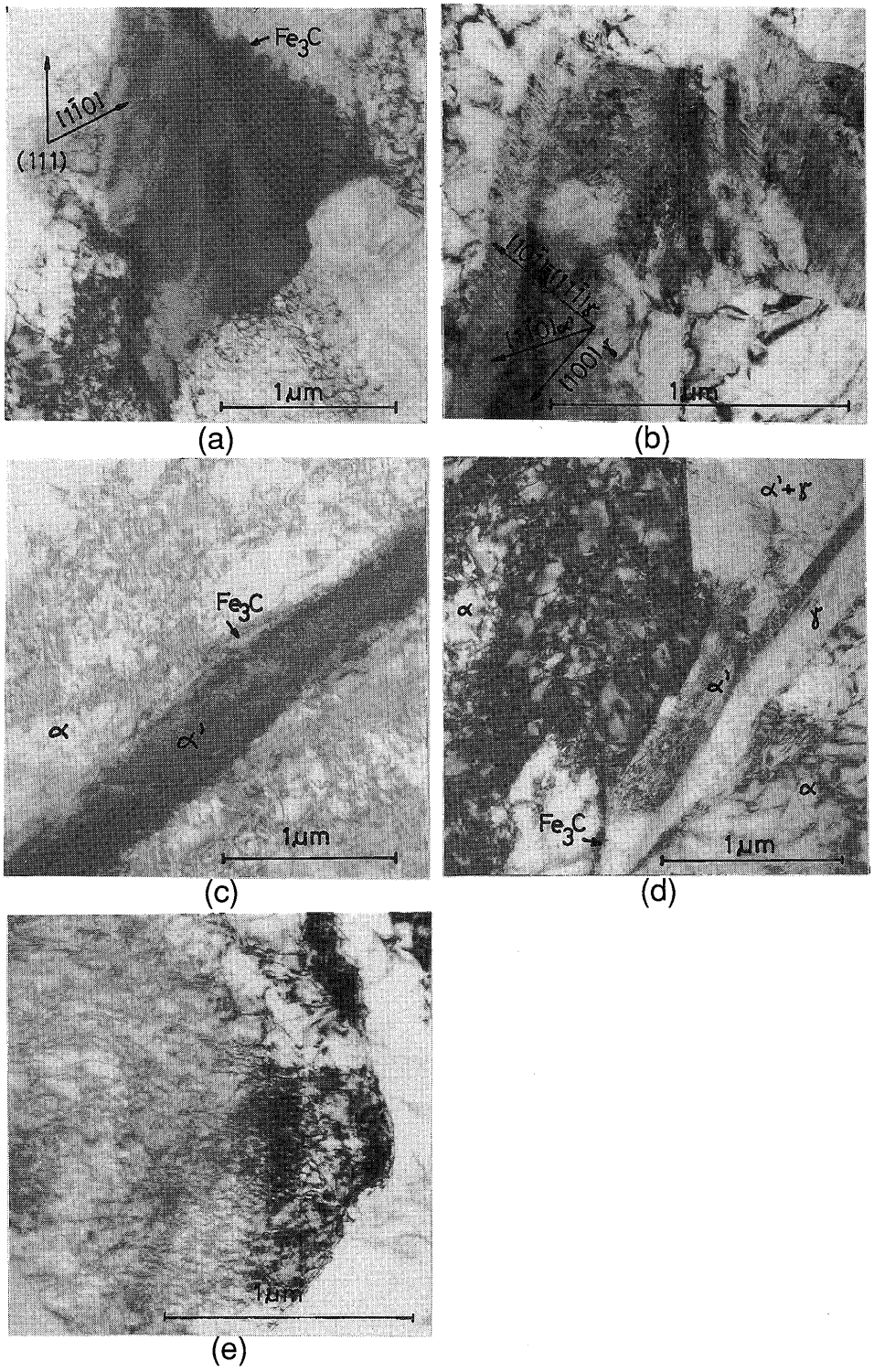

Fig. 6 Examples of M-A constituent morphologies in simulated HAZ of HT 80B (thin foils observed with TEM).

a) massive M-A particle with cementite, lath and plate martensite.

b) massive M-A particle with lath and plate martensite. The plane of foil is $(111)_{\alpha'} // (110)_{\gamma}$.

c) elongated M-A particle with lath martensite.

d) massive M-A constituent with lath and plate martensite, retained austenite and cementite.

e) martensite lath with high dislocation density.

retained austenite was recorded. Retained austenite has a considerably lower dislocation density than surrounding ferrite and is situated either as small islands inside M-A or between the martensite laths. In some cases it was possible to resolve the high dislocation density inside lath martensite (Fig. 6e). Following orientation relationships were found between martensite and retained austenite:

$[111]_\gamma // [1\bar{1}0]_\alpha$,

$[100]_\gamma // [110]_\alpha$,

We have also studied the decomposition of M-A by the heat of next welding pass. Apart from the changes which could occur in the dislocation structure of martensite, we could observe a precipitation of very fine cementite carbides at affecting temperatures over 523 K. An example of the decomposed massive M-A is given in **Fig. 7**. The precipitation of cementite at the boundary between M-A and matrix is more intensive. It is supposed that this stage of M-A decomposition is not improving toughness yet. Only next stage, proceeding at higher temperatures (above ~ 673 K) at which fine cementite particles are re-dissolving and new, coarsened cementite particles are more spread in matrix, is effective for the toughness restoration.

Concerning the transformation temperature of M-A, it was mentioned that its measurement is rather uncertain. An explanation of this may be in the sequence of retained austenite decomposition. The precipitation of cementite from austenite can occur at temperatures 523-773 K. The carbon concentration in retained austenite is so decreased that a part of retained austenite can transform to lath martensite at e.g. 673 K. Other part of retained austenite with higher carbon concentration may transform to plate martensite at considerably lower temperatures (e.g. 473 K). Lath martensite can undergo a self-tempering process, during which fine cementite is precipitated from it. And, finally, some portion of retained austenite may remain untransformed.

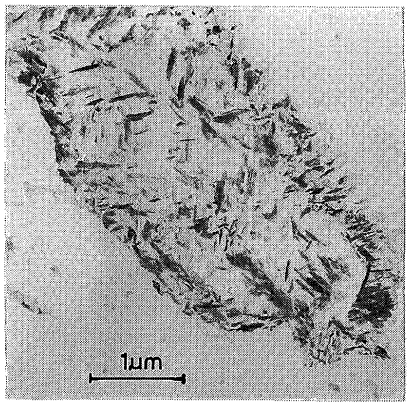

Fig. 7 An early stage of M-A decomposition in HT 80B forming cementite precipitates (extraction carbon replica).

3.2 Behavior of M-A during Straining and Fracturing

The behavior of M-A during straining and fracturing was investigated in slow rate bending tests and impact tests. Bars 10 × 10 mm made from simulated underbead zone of HT 80B were used in both experiments. In bending tests, the bending radius was 20 mm, maximum strain rate 0.3 mms^{-1}, and maximum strain log ϵ = 0.7 on the extended side of the specimen. Deformation was carried out at 5 different temperatures (ambient, 273 K, 253 K, 213 K and 77 K). The behavior of M-A during straining was evaluated on polished and etched specimens taken from the strained area. At room temperature as well as at temperatures down to 213 K the deformation ability of simulated underbead zone was good. At a temperature of solid carbon dioxide (213 K) and liquid nitrogen (77 K), however, the specimens fractured nearly at nil deformation.

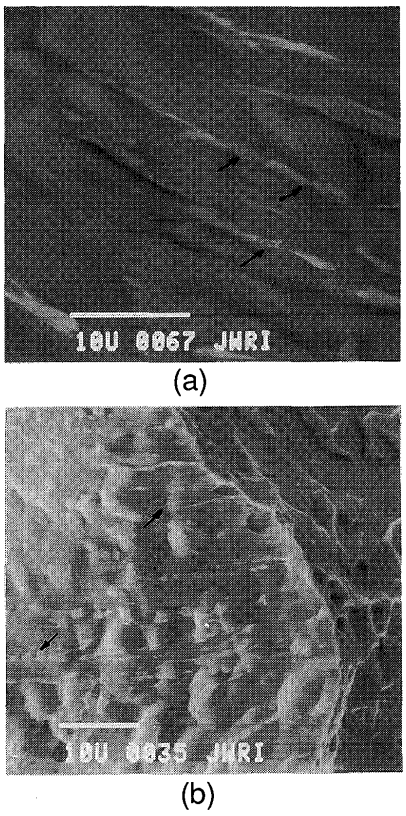

Fig. 8 Examples of M-A behavior during straining. Cracking and fragmentation of elongated M-A constituent (a) and the resulting dimple fracture (b).

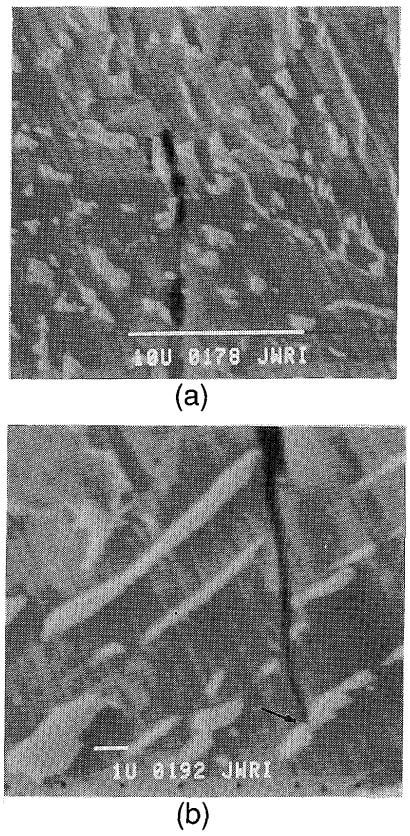

Fig. 9 Initiation of microcracks at both sides of M-A particle.

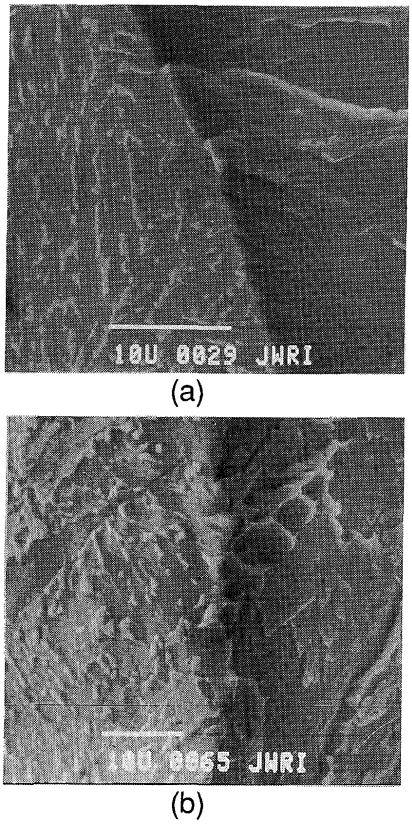

Fig. 10 Examples of contemporary observations of polished and etched surface (left) and corresponding cleavage fracture surface observed with SEM.

In ductile temperature range the usual fracture mode is the initiation of microvoids, their growth and coalescence. A dimple fracture is then the result. Microvoids are initiated at interfaces between the matrix and particles, like inclusions, precipitates, cementite or M-A constituent. The sites where microvoids can initiate may be also some micropores, microcracks, grain boundaries, cleavage planes or slip bands. Coarse grains may concentrate the stress at the end of slip bands and grain boundaries.

As mentioned above we have observed the behavior of M-A particles on the surfaces of metallographic specimens during deformation and fracturing processes. Usually the polished surface was etched prior to deformation. When crack or fracture appeared we could simultaneously observe the etched surface of the specimen, and the corresponding fractured surface because of the high depth of focus of scanning electron microscope observation. It is known that stress triaxiallity is higher inside the specimen than on its surface. Therefore we have prepared metallographic specimens also in the bulk of the strained rods in planes perpendicular to fracture surface. And, finally, to resolve better the configuration of M-A particles on fracture surfaces, fracture surfaces were etched in Nital, too.

Evaluating the results of great many tests we can conclude that in the ductile temperature range the M-A particles exhibited a good straining ability. Only at high strains the particles cracked or were fragmented. **Figure 8a** shows a fragmentation of elongated M-A constituent in heavily strained slip band. Figure 8b was taken near the fracture surface. Fragmentation can be observed in this figure, too. Fractured M-A particles may initiate dimpled fracture. Inside the dimples we could detect M-A particles. By etching the dimple fracture we could not reveal more particles on the fracture surface.

When the temperature of straining was lowered, the straining ability of ferrite was lower and microvoids or cavities nucleated at lower strains than in previous cases. Microvoids and cavities were often nucleated in the ferrite close to M-A boundary. In **Fig. 9a**, an example is given of crack nucleation on both sides of M-A particle. Cleavage crack can either intersect the M-A particles or M-A can act as obstacle for propagating crack. Sometimes particles have kinked-out the propagating cleavage crack from its original path. Figure 9b characterizes such examples.

M-A constituent, as hard second-phase particles, can increase the strength of weld, but at the same time

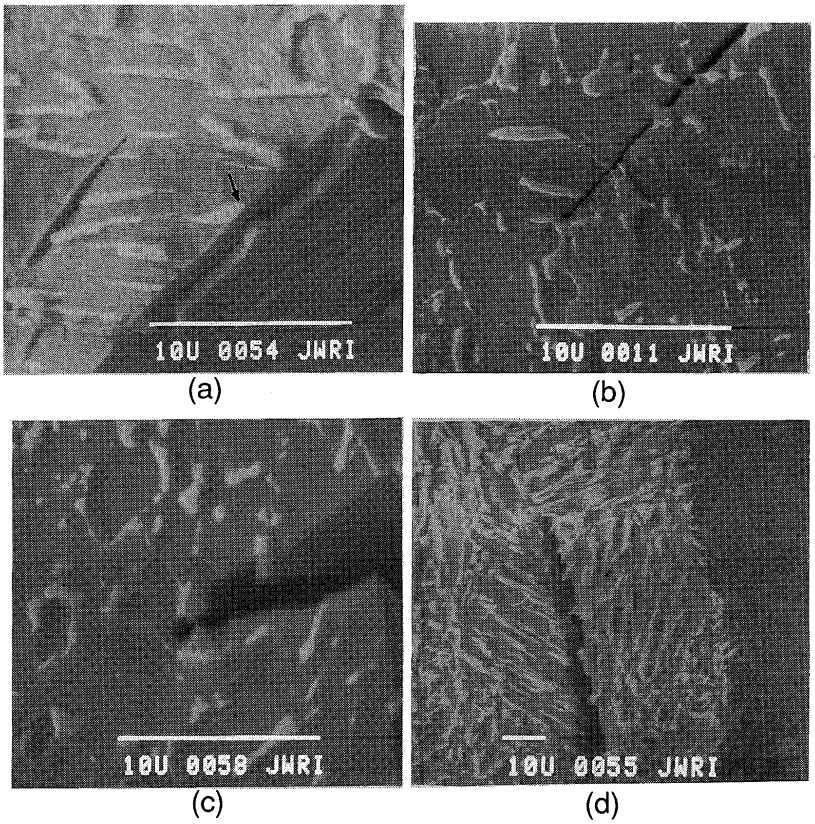

Fig. 11 Secondary cleavage cracks and their interaction with M-A particles (a)-(d).

decrease its ductility by promoting the dimple fracture initiation. Notched rods 10 × 10 mm were used in impact tests, which were done in the same temperature range as bending tests. In the ductile temperature range, the fracture appearance was mostly dimple, and the M-A particles behaved in a similar manner as in bending tests. At ductile-brittle transition temperature (253 K) or below, the fracture mode changed to cleavage. It is generally agreed that the major cause of brittle fracture is inability of the matrix to resist crack propagation through local plastic flow at the tip of the crack. The fracture path followed a transgranular $\{100\}_{\alpha\text{-Fe}}$ plane and changed orientation from grain to grain, resulting in branching of the crack. The river patterns were well developed. The presence of M-A particles was recorded at the edge of river patterns. Higher amount of secondary cleavage cracks was observed also in metallographic specimens prepared from inside the fractured rods. Typical examples of transitions from metallographic microstructure to cleavage fracture are given in **Figs. 10a** and **10b**. Figure 10a shows that when cleavage crack reach M-A particles, a step on the fracture (river pattern) may appear. Sometimes M-A particles were giving rise to quasi cleavage fracture. In **Fig. 11a** also the intersection of M-A particle by propagating crack is seen. Sometimes, cleavage crack was kinked-out by M-A particles (Figs. 11b and 11c). Figure 11d shows etched fracture surface, in which high concentration of M-A particles can be recorded. As seen in **Fig. 12a**, in proeutectoid ferrite no M-A particles are revealed after etching. At the edges of river patterns higher concentration of M-A is detected (Fig. 12b). The elongated M-A particles have predominant orientation $<100>_{\alpha\text{-Fe}}$, which is in agreement with the findings of Pitch and Schrader[13] concerning the preferential growth of cementite. Figure 12c gives an example of the massive M-A particles distribution on cleavage fracture surface. No predominant orientation of massive M-A was found.

The M-A constituent can promote brittle fracture by reinitiation of cleavage fracture. The reinitiating centers are either cracked M-A particles or small cracks at the M-A/matrix interface. The largest effect on brittle fracture should have massive M-A, in which cracks are bigger than in elongated M-A. But at the same time M-A can hinder the cleavage crack propagation and makes steps on the fracture surface.

Some papers stress the important role of residual austenite in fracture propagation[8]. In our experiments the amount of residual austenite was very low (appr. 2%), and therefore we cannot make any conclusion regarding its effect. No doubt that M-A is detrimental to fracture

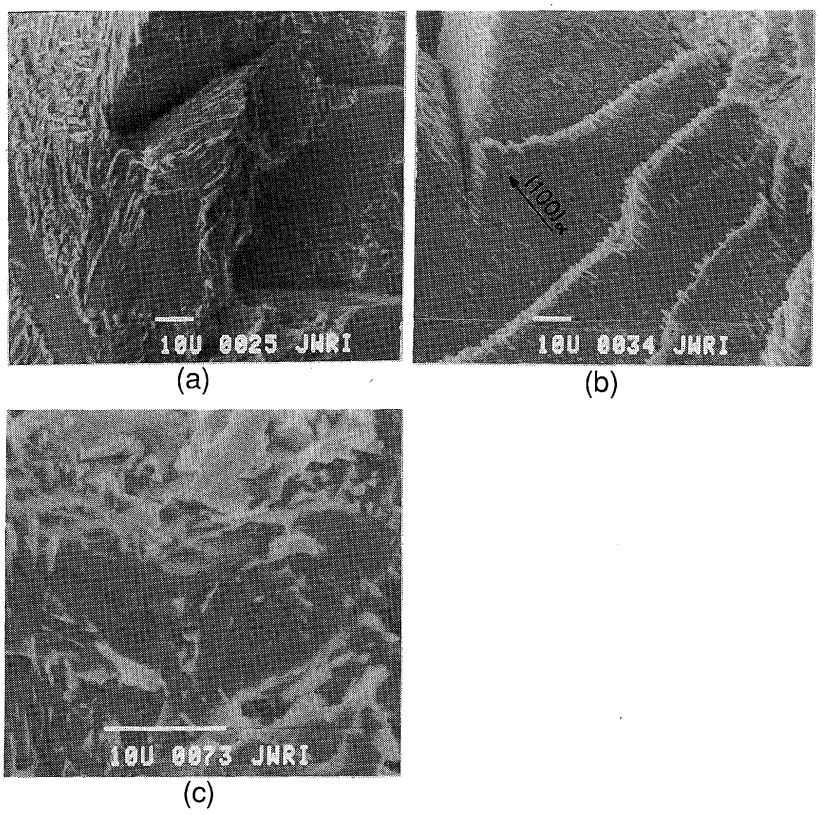

Fig. 12 Examples of M-A on etched fracture surfaces.

toughness. M-A contributes to decrease in upper shelf impact energy. Not so clear is the role of M-A in raising the ductile-brittle transition temperature.

4. Conclusions

1) Concerning the metallography of M-A constituent we have found that the M-A may consist of retained austenite, martensite and cementite. Cementite precipitating from austenite is coarser than cementite resulting from the self-tempering of lath martensite. Two types of martensite were detected both in elongated and massive M-A particles: lath martensite and plate martensite. Retained austenite was found as small islands inside the M-A or between the laths of martensite. The orientation relationships between martensite and residual austenite found by electron diffraction were in agreement with the Kurdjumov-Sachs orientation relationships. In the HAZ of the investigated steels, elongated and massive M-A constituents were found.

2) It is nearly impossible to determine certain transformation temperature for M-A constituent. Cementite can precipitate from austenite at high enough temperatures (e.g. 773 K), the lath martensite can have M_S temperature around 673 K, and plate martensite below 473 K.

3) The decomposition of M-A starts at temperatures above 473 K by precipitation of fine cementite carbides. Complete decomposition of M-A is, however, observed at temperatures above 673 K only.

4) The M-A constituent, as second phase particles, is affecting the ductility and impact properties of weld. In the ductile temperature range, M-A exhibits appropriate straining ability. At higher strains, however, it fractures or even is fragmented. Cracks or fragmented particles can initiate dimple fracture. Microvoids can initiate at the interface between M-A and matrix. By promoting the initiation of dimples M-A lowers the ductility and upper shelf impact energy. In the temperature range of cleavage fracture M-A can contribute to cleavage fracture reinitiation. On the other hand, M-A can hinder the propagation of cleavage fracture by kinking-out the fracture from its original path.

References

1) L.J. Habraken and M. Economopoulos: Transformation and Hardenability in Steels, Climax Mo., Co., An Arbor, (1967)p.69.
2) P. Verrier et al.: Effect of the HAZ Microstructure on

the Fracture Toughness of Offshore Microalloyed Structural Steels, Doc. IIW-IX-1645-91.
3) G.R. Speich and W.C. Leslie: Met all. Trans., **3**(1972)1043.
4) H. Ikawa et al.: J. Japan Weld. Soc., **7**(1977)396.
5) B. Josefsson and H.O. Andren: Proc. Int. Conf. on Recent Trends in Welding Science and Technology, Gatlinburg, Tennessee, (1989), p.243.
6) F. Matsuda et al. : Investigation on the Behavior of M-A Constituent in Simulated HAZ of HSLA steels, Doc. IIW-IX-1591-90.
7) C. Duren: Formulae for Calculating Maximum Hardness in the HAZ of Welded Joints, Doc. IIW-IX-1437-86.
8) T. Terasaki et al.: Proc. Int. Conf. JOM-2, Helsingor, (1984)p.381.
9) N. Yurioka et al.: Metal Constr.,April(1987)p.271 R.
10) G. Krauss: Hardenability Concept with Application to Steels, AIME, Warrendale, (1978)p.235.
11) J.H. Chen et al.: Acta Metall., **32**(1984)1779.
12) F. Matsuda et al.: Trans. JWRI, **20**(1991)69.
13) W. Pitch and A. Schrader: Arch. Eisenhuettenwes., **29**(1958)485.
14) M.F. Ashby and K.E. Easterling: Acta Metall., **30**(1969)1982.